frontiers in Physics

REVIEW
published: 14 May 2020
doi: 10.3389/fphy.2020.00128

Multiphoton Microscopy of Oral Tissues: Review

Rosa M. Martínez-Ojeda[1], María D. Pérez-Cárceles[2], Lavinia C. Ardelean[3], Stefan G. Stanciu[4] and Juan M. Bueno[1]**

[1] Laboratorio de Óptica, Instituto Universitario de Investigación en Óptica y Nanofísica, Universidad de Murcia, Murcia, Spain, [2] Departmento de Medicina Legal y Forense, IMIB-Arrixaca, Facultad de Medicina, Universidad de Murcia, Murcia, Spain, [3] Department of Technology of Materials and Devices in Dental Medicine, "Victor Babes" University of Medicine and Pharmacy Timisoara, Timisoara, Romania, [4] Center for Microscopy-Microanalysis and Information Processing, University Politehnica of Bucharest, Bucharest, Romania

Multiphoton microscopy (MPM) is currently acknowledged as a very powerful method for the visualization and analysis of tissues in biomedicine. It allows high resolution, deep optical sectioning and reduced photodamage. MPM does not require labeling and is deployable both *in-vivo* and *ex-vivo*, which simplifies the diagnostic procedure compared to traditional histology approaches based on excisional biopsy, tissue fixation and staining. Among the important applications of MPM in medicine, differentiation of healthy from pathological tissues has gained massive interest over the past years, but MPM is also very useful for acquiring new insights on how various pathologies originate and progress. In this work we review the use of MPM in imaging assays focused on investigating unlabeled oral tissues (teeth and oral mucosa) and discuss a series of important results which hold potential for enabling a next generation of oral tissue characterization/diagnostic frameworks. The surveyed literature shows that non-linear optical imaging tools can significantly contribute to achieve a better understanding of oral cavity tissues, by allowing the accurate analysis of morphological structures and relevant biochemical processes.

Keywords: multiphoton microcopy, oral tissues, caries, enamel, dentine, squamous cell carcinoma

OPEN ACCESS

Edited by:
Udo Jochen Birk, University of Applied Sciences HTW Chur, Switzerland

Reviewed by:
Susanne Fenz, Julius Maximilian University of Würzburg, Germany
Bernd H. Zinselmeyer, Washington University in St. Louis, United States

***Correspondence:**
Stefan G. Stanciu
stefan.stanciu@cmmip-upb.org
Juan M. Bueno
bueno@um.es

Specialty section:
This article was submitted to Medical Physics and Imaging, a section of the journal Frontiers in Physics

Received: *22 October 2019*
Accepted: *03 April 2020*
Published: *14 May 2020*

Citation:
Martínez-Ojeda RM, Pérez-Cárceles MD, Ardelean LC, Stanciu SG and Bueno JM (2020) Multiphoton Microscopy of Oral Tissues: Review. Front. Phys. 8:128. doi: 10.3389/fphy.2020.00128

INTRODUCTION

The oral cavity represents the first part of the digestive tract, and the main entry for nutrients and different environmental components in the human body. Its main function is to begin the process of digestion by mastication, but speech or breathing are also important functions. Pathologies of the oral cavity can result from a wide range of causes, one of the main sources consisting in harmful components in ingested liquids or food. These may lead either to the genesis of oral diseases or, after being dissolved by saliva and ingested, may cause other minor to major health problems with respect to the gastrointestinal system, and not only. Besides toxic food, tobacco and alcohol, other environmental factors may also be responsible for the occurrence of various oral diseases, ranging from dental caries [1, 2] to oral squamous cell carcinoma [3–5]. In general, all the structures in the oral cavity, including teeth and soft tissues will be at some point affected during one's life by various types of pathologies, or by age related modifications.

Although teeth have a damage resistant structure, this might fail due to environmental factors, diseases or habits. The appearance of cavities may cause pain and other consequent oral problems. However, these are not the most severed pathologies the oral cavity is exposed to. According to current data, half of all cancers in humans appear in the squamous epithelium, which is also lining the soft surfaces in the oral cavity [6]. More specifically, oral squamous cell carcinoma (SCC) represents about 90% of the malignant lesions developed in the oral cavity [7].

At present, various complementary imaging techniques are being used for characterizing hard and soft tissues in the oral cavity, each exhibiting its own strengths and limitations. Since Rontgen discovered radiographs in the late 1800's, radiation was selectively used for the diagnostics and therapy of oral tissues [8]. Periapical and cephalometric radiographs have been used for detecting caries, analyzing bone structures and for planning implantological interventions. Their main disadvantages relate to the interposition of anatomic structures, and the potential harmful effects of the ionizing radiation [9]. Even in latest generation panoramic radiographs, direct ionizing damage and indirect damage from the free radicals created during the ionization of water molecules within cells is associated with a risk of cancer. Computed Tomography (CT), first reported experimentally in the 1970's, combines the concepts of x-ray imaging (performed under different angles) with the advantages of computer technology to provide cross-sectional images of the scanned tissue region, allowing its tomographic inspection [10]. A subsequent technology, Cone-Beam Computed Tomography (CBCT) [11] allows faster acquisition speed and lower radiation exposure, down to 10 times less compared to conventional CT. This diagnostic imaging technology is now widely popular for oral medicine being capable of providing three-dimensional representations of teeth and jaws. Besides limitations in resolution, its main shortcomings are exposure to ionizing radiation (which is reduced, but still exists), and inability to simultaneously image calcified and non-calcified dental tissues, particularly important in regenerative endodontics [12, 13]. Another medical-imaging technique that has been shown to be very valuable for imaging oral tissues is Magnetic Resonance Imaging (MRI), which uses non-ionizing radiation from the radiofrequency band of the electromagnetic spectrum, thus reducing the irradiation hazards that the patient needs to face. MRI can be used for imaging pulp attached to the periodontal membrane, and obviously other soft tissues in the oral cavity. However, it cannot easily visualize teeth because of their high mineral content. Sweep Imaging with Fourier Transformation (SWIFT) [14], an update to conventional MRI, overcomes these limitations, enabling the three-dimensional visualization of both soft and hard (enamel, denting, cortical bone) oral tissues, while also reducing acquisition time [15]. SWIFT-based MRI has the potential to precisely determine the extent of carious lesions and simultaneously assess pulpal tissue [15]. The usefulness of these aforementioned techniques is biased by their limited resolution (lying in the millimeter range). To address this, several safe and non-invasive optical techniques have been introduced to the field of oral tissue imaging over the past couple of decades. Among these, Optical Coherence Tomography (OCT) has successfully been used for the detection and microscale characterization of tooth and periodontal disorders. Applications such as root canal imaging, diagnosis of vertical root fractures, dental microstructure assessment, detection of recurrent caries and loss of marginal integrity of fixed restorations demonstrate its huge potential in dentistry [16–18]. Compared to conventional OCT, Polarization-Sensitive OCT (PS-OCT) [19] provides better resolution and can therefore image also early enamel lesions and secondary caries. It can also be used for the assessment of dentin and cement demineralization and remineralization, representing a useful diagnostic instrument for prevention and early intervention [20]. The resolution achievable with OCT is positioned between the resolution available with ultrasound-based techniques, and with point-scanning optical techniques, e.g., Confocal Laser Scanning Microscopy (CLSM). This latter technique, CLSM, is also well-suitable for *in vivo* clinical studies (in implementations for endomicroscopy), being able to non-invasively provide optical sections of both hard and soft tissues in the oral cavity [21–23]. Importantly, the current gold standard for the diagnostics of soft oral tissues remains the histopathological exam, consisting on brightfield microscopy of tissues that are excised, fixed and stained. However, this approach presents important disadvantages such as long diagnosis time, invasiveness, artifacts, sampling error, time consumption, high costs, and interpretive variability [24–26]. In **Figure 1**, we present a series of images that are representative for these techniques above discussed.

During the past couple of decades, Multiphoton Microscopy (MPM) has emerged as a powerful tool to explore the structure and function of biological samples, and especially of tissues. This is mainly because MPM techniques can non-invasively acquire optical sections (virtual biopsies) in unlabeled tissues, containing information that is very relevant for diagnostic purposes. These non-linear techniques are based on the theory of quantum transition through photons proposed by Nobel Laureate Maria Göppert-Mayer [32], and the first MPM experimental implementation was demonstrated by Denk, Strickler and Webb in Cornell University in 1990 [33]. During the non-linear processes that take place, the sample absorbs two or three infrared photons and emits a unique photon of shorter wavelength. This can occur via different physical processes, that may take place quasi-simultaneously, e.g., fluorescence or harmonic generation, which have been thoroughly discussed in previous reviews [34–36]. The MPM imaging modes are Two-Photon Excitation Fluorescence (2PEF), Three-Photon Excitation Fluorescence (3PEF), Second Harmonic Generation (SHG) and Third Harmonic Generation (THG), all of these being capable to image tissues in a label-free manner, based on their endogenous contrast. The use of infrared light sources allows deeper penetration into the tissues and reduced scattering [37, 38], with reduced photodamage compared to other optical sectioning techniques working in the visible range, such as CLSM [39].

The aforementioned MPM modalities are complementary and provide biological information that is relevant from different perspectives, including morphology, structural organization and cell metabolism. In brief, the energy (i.e., light) released by fluorophores during 2PEF allows the visualization of different biological components, such as elastin, keratin, melanin, nicotinamide adenine dinucleotide (NAD^+/NADH) or flavin adenine dinucleotide (FAD). Selective probing of these autofluorescent tissue components by 2PEF followed by arithmetic operations for distinct signals enable the non-invasive assessment of important information such as cell morphology, size variation of cell nuclei, blood vessel hyperplasia, or inflammatory reaction related aspects [40–42]. 3PEF relies on the

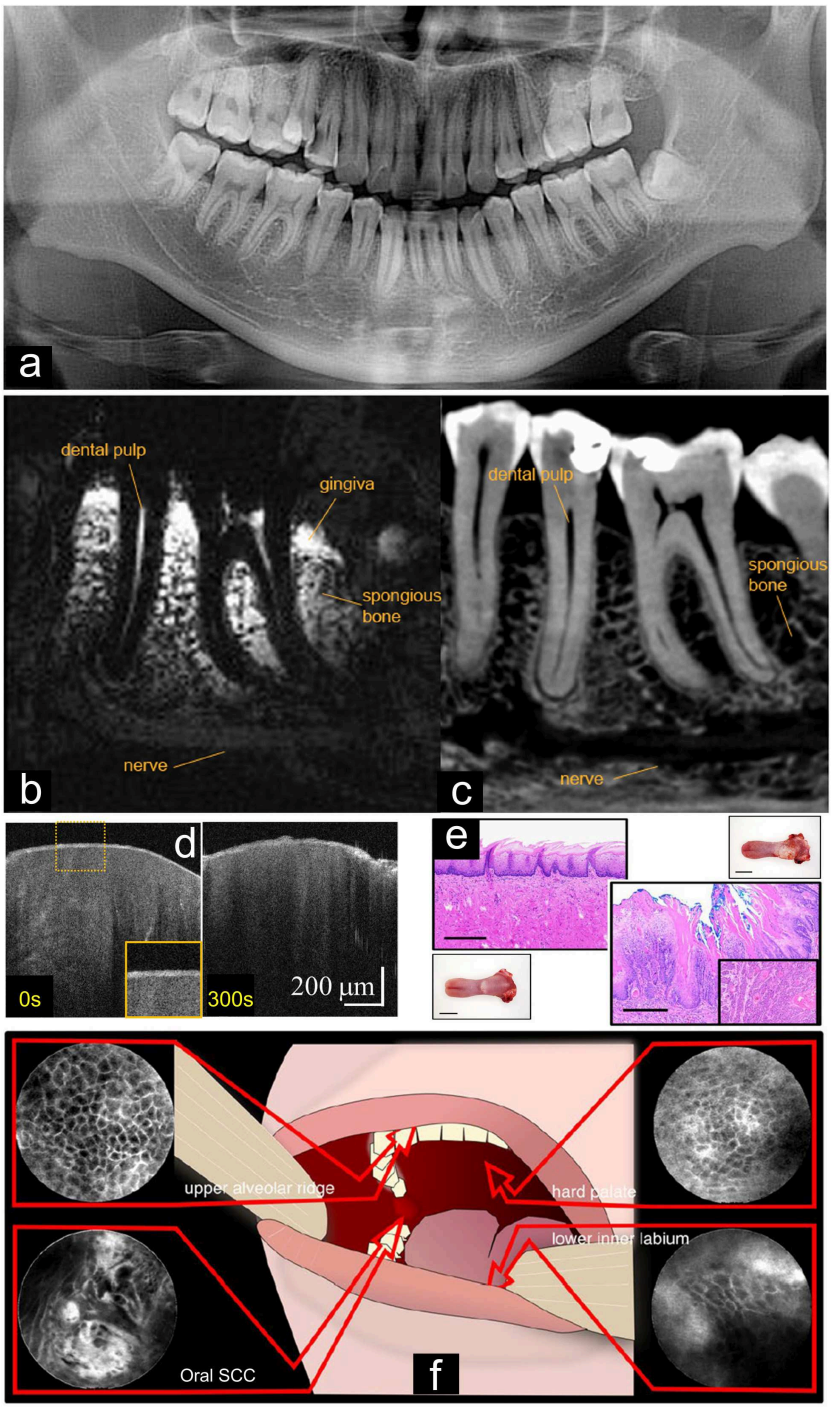

FIGURE 1 | Hard and soft tissues of the oral cavity imaged with routinely used investigation techniques. **(a)** Panoramic dental radiograph. **(b)** Sagital section through MRI and **(c)** CBCT images of the lower jaw. **(d)** Time-series OCT images of a healthy tooth obtained before and after demineralization **(e)** gross observation, and brightfield microscopy images on hematoxylin and eosin (H&E) stained healthy and malignant tongue tissue. **(f)** Confocal laser endomicroscopy images collected on various oral tissues. Artwork reuse permissions: **(a)** adapted from Kim et al. [27], **(b,c)** adapted from Flügge et al. [28], **(d)** adapted from Tsai et al. [29], **(e)** adapted from Kosugi et al. [30], **(f)** adapted from Aubreville et al. [31], all under the Creative Commons CC BY license.

same principles as 2PEF, but usually uses longer laser wavelength to excite the fluorescent molecules, which translates to reduced out of focus light, less tissue scattering, and hence higher penetration [37, 43]. However, 3PEF on tissues is more difficult to achieve and collect, hence related studies are much scarcer compared to the studies that deal with 2PEF imaging of tissues.

We find important to mention here that the potential of 2PEF and 3PEF for probing unlabeled *in-vivo, ex-vivo* or fixed tissues can be further augmented by equipping such systems with time-correlated single photon counting options to enable Fluorescence Life-Time Imaging Microscopy (FLIM) measurements. In addition to the information gained from the intensity of a fluorescent signal, its lifetime provides information on the biophysical environment (e.g., ion and oxygen concentrations, temperature, or pH) of the respective fluorophore [44]. Furthermore, 2PEF/3PEF-FLIM can provide information on a fluorophore's conformational or molecular binding state, whose assessment is also relevant in the context of tissue characterization based on endogenous fluorescence. In a very insightful recent review [45], the authors discuss the importance of FLIM for evaluating cell metabolism.

SHG signals are exclusively originated by non-centrosymmetric structures (e.g., fibrillar collagen, microtubules and skeletal muscle) [35] and THG signal arises from interfaces within the specimen exhibiting a refractive index mismatch [46, 47]. The ability of SHG for probing at high spatial resolution the collagen distribution in tissues facilitates a precise and non-invasive assessment of extracellular matrix modifications specific to various pathologies, enabling consistent diagnostic possibilities [35]. As nicely demonstrated by Kuzmin et al. [48] THG complements SHG, as a result of its ability to image interfaces hosting lipid-rich molecules, allowing thus the visualization of cells and nuclei, or the investigation of vascularization related aspects.

Most MPM imaging studies performed to date on *ex-vivo* and fixed tissues have been performed with tabletop systems, either custom built/modified or commercialized. Such systems can operate in both upright or inverted configurations and require coupling with an appropriate laser source [49]. *In-vivo* imaging on animal models can be done with MPM systems adapted for intravital assays, which require that enough space is available under the objective for positioning the subject of investigation [50].

Most importantly, MPM imaging is also available at present in the form of clinically validated multiphoton tomographs, enabling *in-vivo* assessment of human skin [51]. In addition, a compact non-contact clinically-adapted MPM system has been recently used to image in-vivo the human eye [52]. This implementation offers real-time tissue visualization and the possibility to perform objective analyses of pathological or surgically modified ocular tissues [53–55]. Although, to the best of our knowledge, *in-vivo* imaging has not been yet demonstrated for organs positioned inside the human body (except for exposed brain [56]), recent progress in multiphoton endomicroscopy [57] suggests that such applications are within reach.

Given the advantages above discussed, MPM imaging is likely to become soon one of the default tools for tissue characterization. It can both augment conventional histopathology (e.g., by enabling lower sampling errors), or even replace it entirely in some scenarios. However, there are still challenges on the road to achieving this. For example, interpretation of MPM data can pose problems to histopathologists (who are trained on conventional modalities, e.g., brightfield microscopy of stained tissues). Collecting MPM datasets inside the human body is difficult due to intrinsic tissue movement that cannot be controlled. Non-invasive imaging of deep tissues with MPM is difficult due to light scattering and attenuation. However, despite of all these, there are still many applications where MPM imaging was demonstrated to be very useful. Therefore, MPM is currently regarded as a highly efficient tool for the study of pathological tissues, ranging from epithelial tissues [42], and internal organs [58] to ocular structures [54, 59] or brain tissue [43, 46, 60]. In this article, we review MPM applications focused on the study of oral tissues, addressing previous efforts dealing with visualization and analysis of different structures in the oral cavity, and objective diagnostic methods that were reported to detect and discriminate various oral diseases.

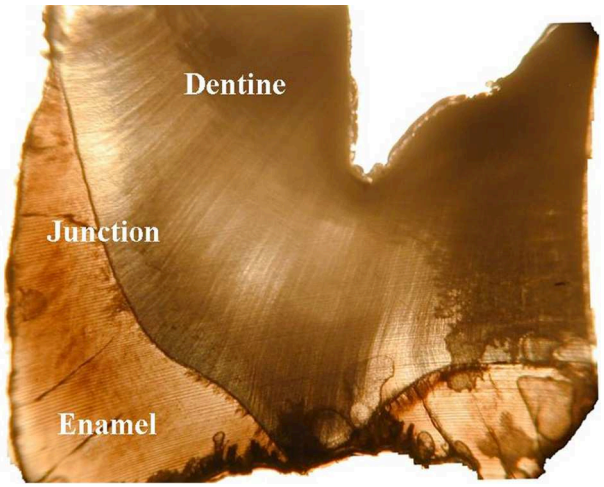

FIGURE 2 | Photo of a longitudinal dental section. Courtesy of Dr. Stephen Chin-Ying, Department of Preventive Dentistry, National University of Singapore. Image size ~4 × 4 mm^2.

MULTIPHOTON MICROSCOPY OF THE TOOTH

Tooth Structure

Enamel, dentine, cementum and pulp represent the structural components of the tooth [61]. An example of a dental section is presented in **Figure 2**.

Enamel is the hard and highly mineralized cover of the tooth crown. It is the most mineralized tissue in the human body, mostly made up of apatite crystals. When the tooth emerges into the oral cavity, ameloblasts (cells that produce the enamel) disappear; for this reason, enamel can't be regenerated. The dentin-enamel junction separates enamel and dentin.

Dentine is also a mineralized tissue, but elastic, avascular, and composed of apatite and collagen. The dentine structure is formed by packed tubules along its entire thickness. Tubules are responsible for tooth hydration and transmission of the physical signals and they are found along the entire structure, running

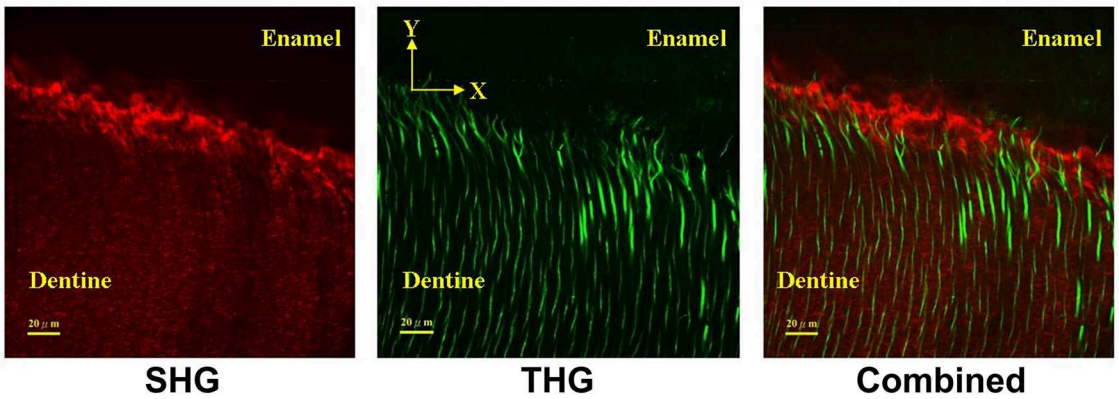

FIGURE 3 | SHG image (in the forward direction) from a location near the dentine-enamel junction (left). THG image from the same location clearly showing the dentinal tubules (center). Superposition of SHG and THG signals (right). It should be noted that the collected THG signals are much weaker compared to the SHG signals and consequently higher incident laser power or higher detector gain was required for image acquisition. Artwork: courtesy of Prof. Fu-Yen Kao (Institute of Biophotonics, National Yang Ming University, Taiwan), images were acquired during the experiment reported in [66].

from the pulp to the enamel and cementum. The diameter and density of the tubules increases toward the pulp [61].

The innermost part of the tooth is the pulp, formed by connective tissue that feeds and regenerates the dentinal collagen through the cells called odontoblasts. Moreover, it is richly innervated with sensory afferents, mostly involved in pain mediation.

The root is the part of the tooth covered by gingival tissue. At this location, dentine is covered by a connective tissue, cementum [62], made of a hard bone-like connective tissue that grows in concentric bands, which increases in thickness throughout life. The cementum also joins the periodontal ligament to the tooth, fixing it to the alveolar bone.

The most common tooth disease is caries, which is characterized by demineralization and degeneration of the organic matrix (i.e., collagen denaturation) [1]. Microorganisms in dental plaque are mainly responsible for caries initiation, but caries have also been related to systemic diseases [63]. Caries affect both enamel (coronal caries) and cementum (root caries) and, in later stages, the dentine or even the pulp.

MPM of Tooth Components

Investigating at high resolution the highly mineralized composition of the tooth typically requires processes of decalcification and staining that may alter its natural structure. This can be avoided by employing MPM to characterize the structure of dental pieces, which has been demonstrated as an important alternative tool.

To our knowledge, Kao et al. in 2000 were the first to report that the tooth generates SHG signal in the back-scattered direction (or epi-illuminated mode), but the details provided for the employed samples were limited. Moreover, the quality of the SHG images presented in that study was low compared to current standards, and probably due to this, the SHG signal was (erroneously) attributed to the highly organized structures of the enamel that encapsulates the dentine [64]. Later, the same group showed SHG and THG images of the dentine in transmission (or forward-scattered) mode [65]. In this second effort the images were acquired in areas near the dentine-enamel junction of a dental section, which allowed observing that the enamel does not generate any of the two considered non-linear signals. Instead, THG images revealed the tubule structure of the dentine, since this kind of MPM signal is sensitive to interfaces and boundaries, while SHG images were found to simply exhibit dentinal collagen content. The absence of SHG in enamel was also confirmed by a wavelength-dependent study [66]. An example of SHG and THG images collected near the dentine-enamel junction are depicted in **Figure 3**.

Non-linear signals from dental structures have also been explored in additional efforts dealing with other MPM imaging approaches. For example, in Chen et al. [67, 68] the authors focused on collecting submicron epi-illuminated MPM images of the enamel, dentine and periodontal ligaments. It was found that enamel exhibits a strong 2PEF signal, revealing the structures of the enamel rods; the dentine presents not only 2PEF signal, but also SHG. It is important to highlight here that the contrast provided by SHG imaging was not only useful to analyze the peritubular dentine structure, but also to distinguish the less mineralized circumpulpal dentine areas that were found to generate only SHG signal, and no 2PEF. That is, the more mineralized the dentinal structure becomes, the higher the 2PEF emission. In addition, due to their dominant collagen-based composition, clear observation of periodontal ligaments was also possible with SHG. The complementarity of SHG and 2PEF signals with respect to imaging hard oral tissues is shown also in **Figure 4** where we present a pair of SHG-2PEF images collected on the dentinal area of a tooth. For a direct comparison they are presented with the same color scale [69]. Noteworthy, the inherent confocality of MPM allows three-dimensional (3D) projections to be built, which facilitates the visualization of interesting features and their placement into a relevant topographic context. In **Figure 5** a 3D reconstruction of the dentine from SHG imaging is shown, and tubules can clearly be observed [69].

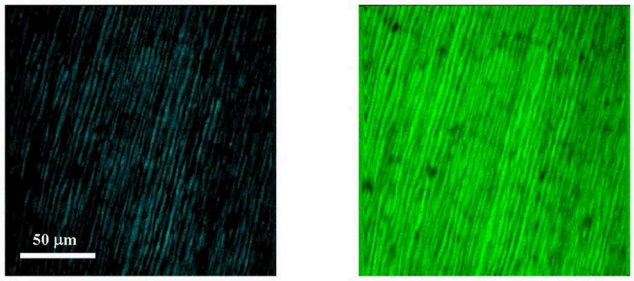

FIGURE 4 | SHG (left) and 2PEF (right) images recorded at the dentine. Since images share the color bar, it can directly be observed how the former is much dimmer compared to the latter. Adapted from Bueno et al. [69].

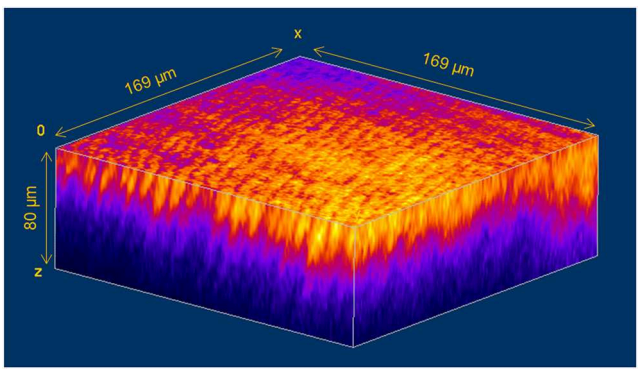

FIGURE 5 | 3D projection of the dentinal area. Adapted from Bueno et al. [69].

Elbaum and colleagues also reported high-resolution 3D images of tooth dentine, but in their experiment this was achieved based on SHG and THG images [70] in the forward-scattered mode. In their quest to explore the architecture of the dentine tubules and the surrounding collagen distribution, they were able to image depth locations up to 200 microns into the sample. The processed 3D reconstructions enabled the visualization of individual tubules and the collagen fibrils mesh around them with an optical resolution of about 1 micron. An important conclusion of their work is that collagen fibrils are organized perpendicularly to the tubules, however close to the dentin-enamel junction they lie also along the long axis of the tubules.

Another experiment, this time dealing with back-scattered MPM, showed that no significant SHG signals can be collected in this configuration on enamel, but THG images successfully revealed its prism structure and distribution [71]. The employed imaging configuration showed stronger THG signal compared to those reported in previous studies performed in transmission [65, 66], allowing thus a penetration depth exceeding 300 µm below the natural tooth surface. It was useful to observe that at the superficial enamel layer, the prisms were found to be organized in a honeycomb structure perpendicular to the tooth surface, and that this direction becomes parallel to the surface as deeper enamel layers are imaged.

In another effort focused on studying the dentin-enamel junction with MPM [72], 2PEF and SHG signals were simultaneously acquired in back and forward directions, respectively. The superposition of image pairs allowed clearly visualizing the junction. It should be noted here that 2PEF images revealed the transitional zone of the enamel as a non-fluorescent irregular line corresponding to the interface between dentin and enamel. This line of dim intensity was associated with very low concentration of protein and hence the lack of endogenous fluorophores. Similar to previous studies, SHG signal was not present in enamel, suggesting an absence of non-centrosymmetric proteins. While enamel prisms were found to exhibit high 2PEF signals, the inner aprismatic enamel (located close to the junction) showed a homogeneous low 2PEF signal. In the same experiment, dentine was observed to provide both SHG and 2PEF signals. The latter was hypothesized to be related to the odontoblast process which involves fluorescent proteins. SHG signals were much weaker compared to 2PEF (see **Figure 4**), what might indicate a low amount of highly non-centrosymmetric molecular assemblies as collagen and microtubules. The dentinal SHG intensity was found however to increase from the junction toward the inner dentine.

The work by Pan et al. took MPM imaging of teeth one step further by addressing tooth morphogenesis [73]. MPM images were used to investigate the development of the tooth in neonate mice from birth to the seventh day after. Results showed that predentina emits solely SHG signal, but dentine structures were observed to provide both SHG and 2PEF. Enamel, odontoblast and ameloblast were also found to exhibit strong 2PEF signal.

Another component of the tooth, dental cementum, has also been analyzed through SHG microscopy by H. Aboulfadl et al. [74]. The work showed that collagen fibers are distributed along two directions: radial (i.e., pointing more or less perpendicularly to the root surface) and circumferential (perpendicular to the radial and oriented parallel to the surface), which we regard as an important finding.

Non-linear multimodal microscopy [75, 76] combining Coherent Anti-Stokes Raman Scattering (CARS) [77], SHG, THG, and 2PEF was able to provide information not only on the tooth structure, but also on biochemical and biomolecular aspects [75]. Multimodal imaging revealed the microtubule structure nearby the dentin-enamel junction, and although CARS did not add extra information to that showed by 2PEF in dentine, this experiment demonstrated that its enhanced optical sectioning capability makes it a useful alternative tool for tooth analysis.

In preparation of future dental tissue engineering, Traphagen et al. [78] demonstrated the ability of MPM microscopy to characterize decellularized and demineralized teeth (while preserving the natural extracellular matrix). 2PEF appeared to be distributed throughout both natural decellularized tissue samples, although it was more prominent in the former. In addition, compared to the decellularized tooth tissue, SHG showed (as objectively measured by means of parameters such orientation index, entropy, and collagen density) higher collagen fiber density, and lower degree of organization in the natural one. Work related to demineralized teeth was also reported

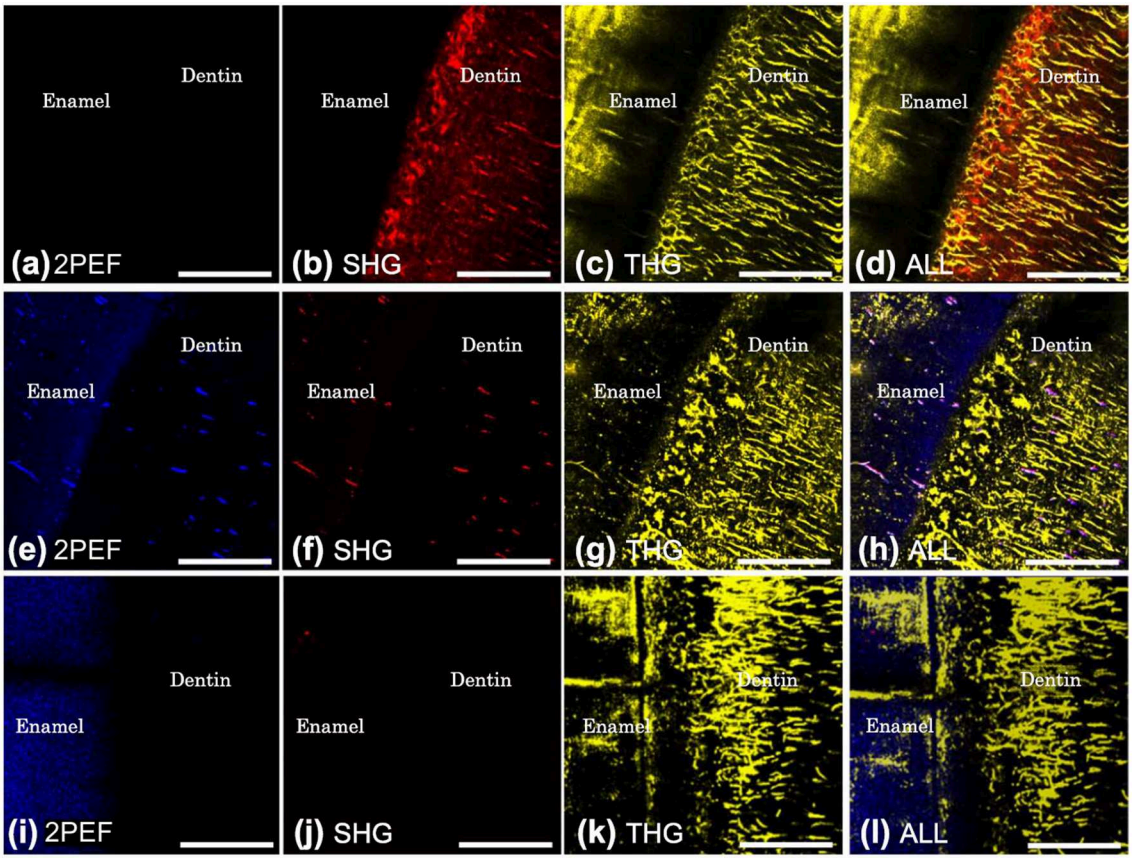

FIGURE 6 | 2PEF, SHG, and THG imaging of extant and fossil teeth of crocodilians. **(a–d)** Images of an extant Alligator tooth acquired under **(a)** 2PEF, **(b)** SHG, **(c)** THG microscopies, and **(d)** overlay of three channels. **(e–h)** Images of a fossil Alligator (1.5 Ma) tooth under **(e)** 2PEF, **(f)** SHG, **(g)** THG microscopies, and **(h)** overlay of three channels. **(i–l)** Images of a fossil Kem Kem crocodilian (93 Ma) tooth under **(i)** 2PEF, **(j)** SHG), **(k)** THG microscopies, and **(l)** 2PEF, SHG and THG overlay. All scale bars, 40 μm. Ma, millions of years. Adapted with permission from Chen et al. [80] © The Optical Society.

by Atmeh et al. [79], where the authors employed 2PEF microscopy to investigate the remineralising potential of certain materials on totally demineralised dentine. Although the signal intensity depended on the sample, these showed microscopic features of matrix remineralisation (including front, intra and intertubular mineralisation).

Most of the previously discussed works propose MPM microscopy as a very valuable tool to characterize various aspects of extant teeth (i.e., extracted teeth from living humans or animals). However, this technique has also been reported to be very useful to explore the anatomy of dentinal tubules in ancient fossil teeth [80]. In particular, THG imaging yielded (unexpectedly) strong signals when dealing with submicrometer level anatomy. When compared to extant teeth, the visualization of fossilized dentine tubules revealed a strong morphological correlation, confirming that the dentinal tubule structures have remained relatively constant through time. This is illustrated in **Figure 6**, which also very nicely demonstrates the complementarity of the 2PEF, SHG, and THG signals for teeth imaging, in general.

MPM for the Analysis of Dental Diseases and Abnormalities

Enamel covers the tooth crown and protects the inner tissues from bacterial infection, as well as from mechanical, thermal, and chemical attacks. Any disorder of this most external dental structure may allow acids and bacteria to penetrate into the inner tissues, which can lead to dental diseases. In the previous section of the manuscript we reviewed published works that aimed to explore sources of non-linear optical contrast in the tooth and the way they can be used to document various properties of this structure. In this part, we review additional work that focused on analyzing dental abnormalities and diseases, such as caries.

Girkin et al. were among the first to report an MPM image showing early dental caries in an intact tooth and proposed MPM techniques as a diagnostic tool in dentistry [81, 82]. In a different effort, MPM microscopy allowed imaging the tooth from the outer part up to a depth of ∼500 microns [83]. The imaged lesion depths compared well with the depths measured by physically sectioning the teeth. While healthy tooth tissue exhibits strong 2PEF signal, as discussed also in the previous section, this is available to a lesser extent in carious tooth tissue [84]. Caries

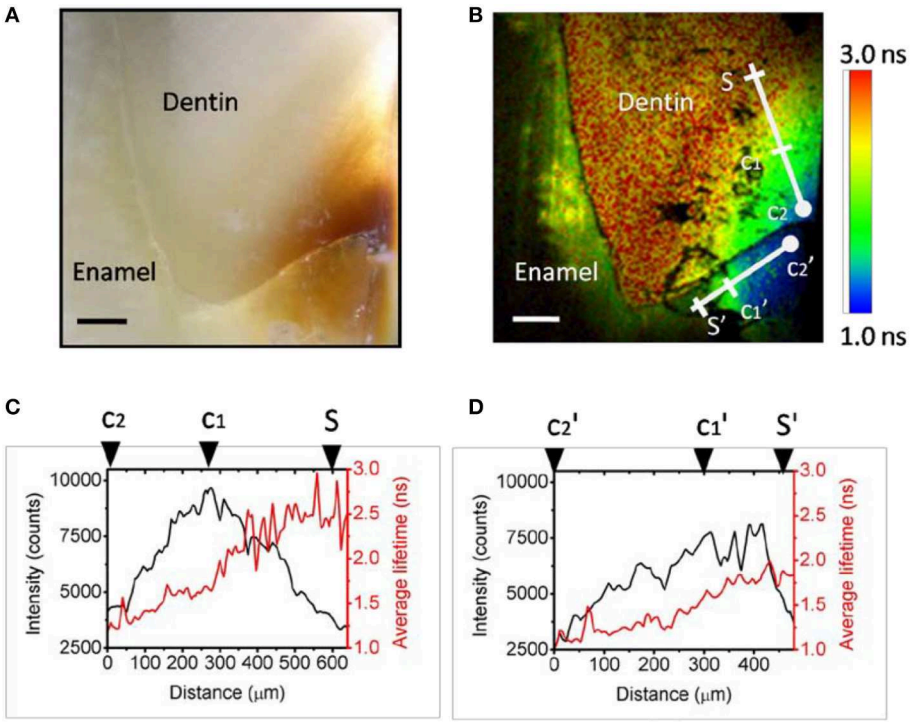

FIGURE 7 | 2PEF-FLIM of dental tissues. **(A)** An epi-illuminated image of the investigated carious dental sample. **(B)** The corresponding 2PEF-FLIM image showing carious regions with greatly reduced lifetime (blue) compared to healthy regions. The scale bar is 200 μm. The intensity (black) and average lifetime (red) line profiles are obtained from the 2PEF-FLIM image depicted in **(B)**, for **(C)** dentin and **(D)** enamel, respectively. Reprinted with permission from Lin et al. [85] © The Optical Society.

appear as a dark spot within a brightly fluorescent tooth, so in a 2PEF inverted image these will appear bright within a dark background, hence the decayed tissue can be well-highlighted with this imaging modality.

In another interesting work, the surfaces of teeth with abnormal enamel were studied and compared to the surfaces of intact human teeth as a basis for future clinical applications [71]. The investigated samples included white spot lesions, cracks, and the artificially-lased (irradiated) enamel. Since prisms within dental enamel present a homogeneous structure of hydroxyapatite crystals, the detected THG signal was thought to originate from the organic-matrix-filled interprismatic space rather than from inorganic crystalline regions inside the prisms. In diseased enamel crystal inhomogeneity appears, and this abnormality reflects in THG signals generated inside the prism. It was hypothesized that white spot lesions are mainly caused by mineral loss (with presence of crystal inhomogeneity), and the THG images collected in this study were coherent with this assumption, depicting different degrees of mineral loss. Moreover, unlike in sound enamel, SHG signal was also found in teeth regions harboring white spot lesions, which is believed to occur due to a symmetry breakage taking place under certain strain. In general, natural cracks may be a result from mechanical damages, thermal stress, and the stress-strain around the cracks; the MPM images were in agreement with this hypothesis. As expected, SHG signals depicting strains originated at the sites of the cracks. In addition, THG images revealed both the cracks and the enamel prisms beside them. Finally, in irradiated human tooth enamel, THG images collected on superficial layers revealed heat-induced cracks. The THG signals originating from the interprismatic space were observed to drastically decrease due to the melting of this superficial layer that takes place during irradiation. The strain at the cracks was also present in SHG images, and both THG and SHG signals were observed around the heat-induced cracks. At deeper locations (with reduced energy absorption and lower prism melting effects) strain sensitive SHG signals were found to become weaker but THG generated from the interprismatic spaces recovered.

In other works, focused on investigating how MPM signals can be used to indicate the tooth's health state, Lin and colleagues confirmed previous results on dental MPM sources and used fluorescence lifetime analysis to differentiate normal dental tissues from caries [85]. The latter were found to present a noticeable decrease in the lifetime of present endogenous fluorophores in both enamel and dentin (**Figure 7**). These results suggest that 2PEF-FLIM's usefulness for identifying carious tissues based on their specific fluorescence lifetime signatures represents an important asset that can potentially augment the current ways of identifying and assessing early sub-surface lesions that can be linked to teeth degradation during carries development. Terrer et al. tackled a similar problem as well and demonstrated that SHG and 2PEF intensities of human dentine were strongly modified during the tooth caries process, as a result of the degradation of the dentinal organic matrix [86].

In addition, they proposed the SHG/2PEF ratio as a reliable parameter to follow dental caries. The usefulness of combining these two complementary MPM signals for detection and classification of carious stages has been recently demonstrated by Slimani et al. [87], who correlate the SHG/2PEF ratio (which they regard as an indicator of the organic matrix denaturation) with the International Caries Detection and Assessment System (ICDAS).

Other important MPM efforts were focused on addressing endodontic infections. The elimination of microbes from the infected root canal system is currently completed by specific medication, but the effectiveness of the disinfection may be limited by microorganisms present in the dentinal tubules. In this sense, ZnO and TiO_2 nanoparticles represent relevant therapeutic agents, given their photoactive and bacterial inhibiting properties. Trunina et al. proposed to use MPM microscopy to visualize the penetration of these nanomaterials in the human tooth tissue [88, 89], in the frame of an *in-vitro* study. While ZnO nanoparticles produced SHG signal, TiO_2 generated 2PEF. Using these two imaging modalities it was observed that ZnO particles penetrate up to 45 microns into the enamel and dentine, respectively, while TiO_2 nanoparticles only penetrated 5 microns. This study suggested thus ZnO as a more promising material for penetration imaging, indicating also that dentinal permeability is one order of magnitude higher than that of enamel (for these types of particles).

Another aspect investigated with MPM was mineral density in the dentine collagen and enamel, which was shown to increase with age [61]. In light of this, a number of methods are emerging to estimate the age of an individual based on the tooth's composition [90]. Bueno et al. have recently reported results on this idea, by using MPM signals as an aging indicator [69]. The procedure relies on exploiting collagen denaturation with age and combines SHG and 2PEF images collected on dentine. The usefulness of such approaches is especially important in forensics, as they can characterize and help identify corpses that have been submerged in water or exposed to high temperatures as a consequence of natural disasters.

MULTIPHOTON MICROSCOPY OF THE ORAL MUCOSA

Oral Mucosa

The oral mucosa is formed by two layers, epithelium and connective tissue [7], and divided into three categories: masticatory (keratinized epithelium), lining (non-keratinized epithelium) and specialized mucosa. The mucosa surrounding the teeth (gingiva), due to its permeability, may be easily passed through by antigens.

One of the major diseases of the oral mucosa is cancer. The golden standard for the diagnostics of this pathology consist in biopsy under general anesthesia, combined with histopathological analysis of the excised tissue following fixation and staining. This method is very useful to evaluate histochemical and morphological changes in the tissue. However, it is subjected to the well-known disadvantages of traditional histopathology, which we discussed in the Introduction. These issues can be overcome or alleviated with the help of fluorescence spectroscopy [91] and MPM [6, 92–94], which have been demonstrated over the past years as very useful non-invasive tools to explore the oral mucosa.

Multiphoton Microscopy of the Oral Mucosa

One of the most important capabilities of MPM consists in its efficiency to characterize the structure and composition of tissues based on the fluorescence of endogenous fluorophores, which has also been demonstrated in the case of the oral mucosa. For example, Wu and collaborators found that 2PEF signals from NADH and FAD in the epithelium can be achieved with an excitation wavelength of 810 nm [95]. These autofluorescence signals are closely linked to cellular metabolism, and their ratio (known as the metabolic redox ratio) has been demonstrated in several landmark studies to reveal metabolism aspects unavailable with other techniques [41, 96]. The authors reported as well-significant SHG signals in the stroma, which were proposed as a sensitive indicator to separate the epithelial layer from underlying stroma. SHG intensity depends on the content and organization of the collagen fibers within the tissue [35, 40, 97], and in the case of the oral mucosa stroma these were highly organized, leading thus to consistent SHG signals. In a different study, Zhuo et al. used MPM to obtain images of the elastin fibers in the oral mucosa [98], and similar to the previous publication, they reported NADH and FAD autofluorescence in the epithelium under 810 nm excitation (however, the 2PEF signal corresponding to NADH was found to be higher at 730 nm). They also found significant SHG signals arising from the stroma and took SHG image analysis one step forward by quantitatively studying the distribution of the collagen (based on both number of fibers and inter-space measurements). In addition, they were able to acquire images and study the morphology of salivary glands, which are surrounded by collagen. MPM signals achieved from NADH, FAD, and collagen were also found to be important in light of their potential utility as biomarkers in the precancerous development of the epithelium [95].

In vivo MPM (yielding virtual biopsies) has also been demonstrated in the human oral mucosa [99]. Images of the epithelium and the lamina propria (connective tissue lying beneath the epithelium) were recorded without producing any damage. The performed measurements lasted about 30 min and the deepest imaged plane was located at 280 μm, which proposes MPM as an important tool for diagnosing pathologies of the mucosa *in vivo*.

Other studies that we find important to mention were focused on characterizing the vocal folds, which are located inside of the vocal tract and vibrate due to the air exhaled by the lungs to originate one's voice. Any problem in the vocal folds might limit the phonation mechanism and hence the treatment of

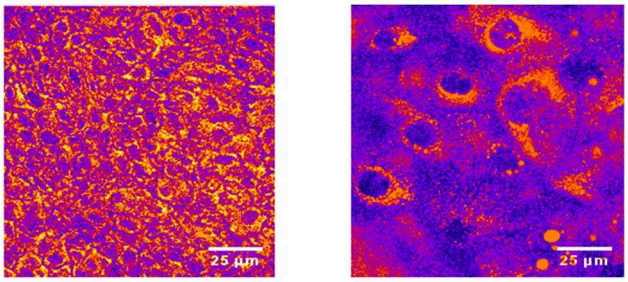

FIGURE 8 | 2PEF images of normal (left) and cancerous (right) tissues. These MPM images are courtesy of Prof. Nirmala Ramanujam (Duke Cancer Institute, Duke University) and Dr. Melissa C. Skala (Dpt. Biomedical Engineering, University of Wisconsin-Madison). They take part of the image set acquired and classified during the experiment reported in Skala et al. [6].

specific diseases, such as nodules and polyps, and requires thus immediate attention. Diagnosing such pathologies requires efficient detection, accurate location and, after surgery, reliable monitoring. In 2012, MPM was proposed as a tool for diagnosis and monitoring of diseases in the vocal folds [100]. Both the extracellular matrix and their overall morphological structure were studied by complementary MPM modalities. SHG and 2PEF images showed the geometry of the collagen and the elastin within the lamina propria, respectively. Two other MPM studies were focused on analyzing the healing process of the vocal folds [101, 102], and very recently, a system combining MPM and nanotomography has been successfully used for their 3D restoration [103].

In a different type of contribution compared to the rest discussed in this section, Sriram et al. [104] have recently introduced a step-by-step MPM imaging and sample preparation protocol for the non-invasive and label-free imaging of monolayer and three-dimensional organotypic cultures of the skin and oral mucosa.

Multiphoton Microscopy of Oral Mucosa Pathologies

Oral SCC originates from a mutation and an uncontrolled proliferation of keratocytes (located in the epithelium of the oral mucosa) [105]. Epithelial dysplasia precedes SCC and involves microscopic changes in the stratified squamous epithelium [106]. According to Vargas et al. [92], the stages of epithelial dysplasia are classified into: mid (dysplastic cells are found in the basal layer of the epithelium), moderate (dysplastic cells are extended through epithelium) and high dysplasia (where cell invasion occupies a large fraction of the epithelium). In carcinoma *in situ* the entire epithelium is covered with dysplasia. In oral SCC there is an alteration of the basement membrane due to invasive cells entering the collagen-based stroma. As an example, **Figure 8** depicts representative MPM images of tissues diagnosed as normal and cancerous.

In 2004, Wilder-Smith et al. explored the feasibility of MPM to act as an efficient tool for oral SCC early detection, and to represent a non-invasive (and faster) alternative to traditional diagnostic approaches that involve biopsy [93]. A variety of relevant structures were clearly noticeable in the images they collected in an *in vivo* hamster model. Also, an important finding of their study was the gradual reduction of the collagen fibers and a loss of the collagen's normal structure. The achieved results were in agreement with traditional histopathological assays that require biopsy, tissue fixation and staining. Later, the same authors combined MPM and OCT to increase the effectiveness of non-invasive oral SCC diagnostic (also in a hamster model) [94]. In this study, blood vessels, epithelial and subepithelial layers, the basement membrane and even the epithelial invasion were imaged by means of OCT, while the structure of collagen and elastin fibers, as well as the vessels, were visualized with MPM. This approach was demonstrated as being very useful with respect to the aimed purpose, and MPM signals were found to be very valuable for following (and understanding) the carcinogenesis process based on changes in the collagen matrix, organization loss, and reduction in length and number of collagen fibers. In a more recent experiment, Elagin et al. [107] showed in an animal model (7,12-dimethylbenz[a]anthracen (DMBA)-induced hamster oral carcinoma) that the complementarity of MPM and OCT can also be exploited for efficiently distinguishing *in vivo* between benign papilloma and papilloma that are either dysplastic or affected by SCC. While the MPM images presented in this study allowed extracting important cellular features such nuclear-cytoplasmic ratio or nuclear density, OCT was demonstrated to provide microvascular maps which were also useful with respect to assessing the pathological state of the characterized tissues.

In a different effort, this time dealing with a mouse model, a protocol combining an established carcinoma model with MPM imaging was used to quantify the invasion of tumor cells; a multi-vectorial visualization of lingual tumor spread was reported [108]. The incorporation of a spectroscopic system into an MPM device also provided interesting results concerning the detection of oral SCC at different precancerous stages. Autofluorescence signals were found to decrease in dysplastic hamsters and furthermore, the *in vivo* emission spectrum showed differences as a function of depth and excitation wavelength, in mid, moderate/high grade dysplasia animals compared to normal ones [109]. The accurate evaluation of the 2PEF spectral characteristics also enabled the identification of unique signatures that can be used to delineate normal oral mucosa from neoplasia [110]. In another study addressing oral carcinogenesis in hamsters, 2PEF and SHG signals showed a significant increase in the epithelium thickness and changes in the morphology and distribution of the keratocytes during different stages of the addressed pathology [92]. Skala et al. also found a similar increase occurring in the epithelium thickness, as well as in the keratin layer thickness [6].

In order to increase the performance of MPM imaging of oral mucosa tissues, the use of gold nanorods for targeting cancerous cells was proposed and demonstrated in an animal model with induced oral SCC [111, 112]. Gold is an inertial biocompatible material and the nanorods require low beam power to be excited. Injected gold nanorods reduced the background of 2PEF images and enhanced contrast. In addition, these particles were also shown to allow improved 3D reconstruction of the vessels [113].

Besides studies on animal models, MPM imaging of oral cancerous tissues was also carried out in humans. Tsai et al. performed an *ex vivo* MPM study on the cancerous mucosa of patients with oral SCC [114]. MPM revealed additional histopathological features compared to traditional histology (irregular epithelial stratification, cytological abnormalities and basement membrane interruption, among others), demonstrating thus the added value of such diagnostics assays. The authors reported changes in the patterns of collagen fibers and in the size and nuclei morphology of the parenchymal cells from SCC tissues. In addition, compared to normal mucosa, actin filamentous structures were more abundant in tumor cells, and an increased damage in the squamous epithelium was found. Also in a human model, Cheng et al. used in 2013 an intravital multi-harmonic microscope to image oral SCC [115]. SHG and THG signals of *in vivo* human tissues were acquired, and SHG microscopy was found useful to image the distribution of the collagen fibers in the lamina propria, whereas THG provided information about the keratocytes present in the epithelium and on the red blood cells in the capillaries.

In other studies, NADH and FAD fluorescence lifetime changes have also been reported in oral SCC tissues relative to healthy tissues, in both living and *ex vivo* experimental conditions [96, 116–118]. As discussed in the introductory part, FLIM relies on the measurement of the time it takes for an excited fluorophore to return to its ground state. This technique was found to be a valuable tool to extract information about the glycolysis and the oxidative phosphorylation in the cellular metabolism [117]. A decrease in the NADH fluorescence lifetime (averaged over the entire epithelium) was found in precancerous compared with normal tissues. On the opposite, a FAD lifetime (averaged) increase was observed in precancerous tissues [96]. However, intracellular variability of NADH and FAD fluorescence lifetimes was found to increase when comparing precancerous and normal cells. These results can be used in identifying cues that precede oral SCC. Furthermore, time-resolved 2PEF images were minimally affected by tissue morphology, endogenous absorbers, and illumination [117], which can significantly increase the robustness of MPM diagnostic assays. In the work of Teh et al. [118], a reduction in the lifetime of NADH fluorescence was found to occur in precancerous tissues compared with healthy tissues. While 2PEF intensity (excitation wavelength, 745 nm) of collagen increased in precancerous tissues, SHG signal decreased. The 2PEF/SHG ratio was found to be higher in precancerous tissues compared to healthy ones, a finding that is also useful for diagnostic purposes. Changes in 2PEF signals corresponding to tryptophan were also shown in different layers of dysplastic epithelium, which can contribute to a better understanding on how cancers of the oral mucosa originate.

Noteworthy, recent efforts have showed that MPM imaging can be significantly augmented by emerging techniques in artificial intelligence. For example, Huttunen et al. have recently demonstrated that MPM images collected on transversal fragments of epithelial tissues can be classified with high precision as being healthy or dysplastic by using a deep learning method that does not require extensively large training datasets [119]. Such methods can play an important role in facilitating the spread of MPM modalities in clinical settings to enable novel non-invasive *in vivo* diagnostic applications, including those potentially addressing oral tissues. This will be further facilitated by deep learning methods developed for virtual staining. Such methods enable the representation of images collected based on endogenous contrast (and not only) to the color schemes most familiar to histopathologists [120], which is also likely to bring significant added value to forthcoming clinical MPM imaging applications addressing oral tissue assessment and diagnostics.

CONCLUSIONS

The aim of this work has been to review previous studies focused on applying MPM to better understand oral tissues and to develop related applications, placing main attention on MPM imaging of dental pieces and oral mucosa, in both healthy and pathological conditions.

Although teeth are made of different types of tissues, the complementarity of available MPM techniques allows observing in detail these distinct structural regions. 2PEF signals originating from cellular constituents provide morphological and functional information. Both enamel and dentin emit strong 2PEF signal, helping to reveal various relevant features in detail (such as enamel prisms and dentinal tubules). Even though the spectral profiles of these signals are similar, they can be differentiated by lifetime analysis. 2PEF emission in the dentine tubules is thought to be associated with the odontoblast process containing fluorescent proteins. 2PEF intensity will vary due to protein content variation.

THG signals arise from interfaces with an abrupt change in the index of refraction. In the case of tooth imaging, this type of signal revealed the fine prism structure of the enamel (interprismatic spaces) but could only be detected in the back-scattered imaging direction. Unlike in enamel, both forward and backward THG images can be acquired on the tooth dentine. THG images showed the dentinal microtubule structure as a result of the sensitivity of THG signals to structural boundaries. While THG provides contrast for the observation of the tubules, SHG can be observed throughout the dentine, due to highly crystallized (and non-centrosymmetric) non-mineral organic matrix based on collagen fibrils.

It is also important to highlight that previous work showed that MPM imaging can be used to explore dental caries and abnormal enamel. Morphological and biochemical modifications suffered by teeth can be characterized by combining different non-linear signals, proposing MPM as a tool capable of significant clinical applications oriented toward the evaluation of dental diseases.

MPM's utility for the characterization and diagnostics of oral tissues has also been demonstrated in a series of important studies focused on imaging soft tissues, both healthy and pathological (mainly oral SCC), at high optical resolution and at different depth locations. In soft oral tissues, 2PEF, SHG, and THG allow the visualization of morphological structures, such as keratocytes, collagen, erythrocytes, and monitoring tissue modifications that occur due to various pathologies. We also find important to

mention that 2PEF lifetime imaging of the NADH and FAD endogenous chromophores provides inestimable information about the metabolism state of the tissue, contributing thus to the potential of MPM for monitoring changes produced in living oral tissues during the progression of various pathologies, including cancer.

In summary, the findings reviewed herein suggest that MPM represents a valuable tool for the *ex-vivo* and *in-vivo* characterization of hard and soft tissues of the oral cavity. With respect to soft tissues, the diagnosis of cancers is the most widely addressed problem so far, but other pathologies specific to the oral cavity could equally benefit of the advantages offered by MPM modalities. Furthermore, the field of dentistry can also take profit of MPM's valuable contrast mechanisms, exploiting these for the diagnostics of early caries and for the accurate visualization of enamel abnormalities.

AUTHOR CONTRIBUTIONS

JB and SS defined the structure of this review and identified relevant works. RM-O and JB wrote the initial version of this manuscript. SS, MP-C, and LA revised the manuscript and incremented on top of the initial version. All authors read, revised, and approved the final version of the manuscript.

FUNDING

JB acknowledges the support of the Fundación Séneca - Agencia de Ciencia y Tecnología de la Región de Murcia (grant 19897/GERM/15). SS is thankful for the financial support provided by the Executive Agency for Higher Education, Research, Development and Innovation Funding (UEFISCDI) via grant PN-III-P1-1.1-TE-2016-2147 (CORIMAG).

REFERENCES

1. Selwitz RH, Ismail AI, Pitts NB. Dental caries. *Lancet*. (2007) **369**:51–9. doi: 10.1016/S0140-6736(07)60031-2
2. Pitts NB, Zero DT, Marsh PD, Ekstrand K, Weintraub JA, Ramos-Gomez F, et al. Dental caries. *Nat Rev Dis Prim*. (2017) **3**:17030. doi: 10.1038/nrdp.2017.30
3. de Camargo Cancela M, Voti L, Guerra-Yi M, Chapuis F, Mazuir M, Curado MP. Oral cavity cancer in developed and in developing countries: population-based incidence. *Head Neck*. (2010) **32**:357–67. doi: 10.1002/hed.21193
4. Mello FW, Melo G, Pasetto JJ, Silva CAB, Warnakulasuriya S, Rivero ERC. The synergistic effect of tobacco and alcohol consumption on oral squamous cell carcinoma: a systematic review and meta-analysis. *Clin Oral Investig*. (2019) **23**:2849–59. doi: 10.1007/s00784-019-02958-1
5. Jiang X, Wu J, Wang J, Huang R. Tobacco and oral squamous cell carcinoma: a review of carcinogenic pathways. *Tob Induc Dis*. (2019) **17**:1–9. doi: 10.18332/tid/111652
6. Skala MC, Squirrell JM, Vrotsos KM, Eickhoff JC, Gendron-Fitzpatrick A, Eliceiri KW, et al. Multiphoton microscopy of endogenous fluorescence differentiates normal, precancerous, and cancerous squamous epithelial tissues. *Cancer Res*. (2005) **65**:1180–6. doi: 10.1158/0008-5472.CAN-04-3031
7. Massano J, Regateiro FS, Januário G, Ferreira A. Oral squamous cell carcinoma: review of prognostic and predictive factors. *Oral Surg Oral Med Oral Pathol Oral Radiol Endod*. (2006) **102**:67–76. doi: 10.1016/j.tripleo.2005.07.038
8. Mupparapu M. Diagnostic imaging in dentistry. *Dent Clin North Am*. (2016) **60**:xi–xiii. doi: 10.1016/j.cden.2015.10.001
9. Brenner DJ, Doll R, Goodhead DT, Hall EJ, Land CE, Little JB, et al. Cancer risks attributable to low doses of ionizing radiation: assessing what we really know. *Proc Natl Acad Sci USA*. (2003) **100**:13761–6. doi: 10.1073/pnas.2235592100
10. Whitehouse RW. Computed tomography. In: Cassar-Pullicino VN, Mark Davies A, Editors. *Measurements in Musculoskeletal Radiology*. Berlin: Springer Berlin Heidelberg (2008). p. 15–29.
11. Sukovic P. Cone beam computed tomography in craniofacial imaging. *Orthod Craniofacial Res*. (2003) **6**:31–6. doi: 10.1034/j.1600-0544.2003.259.x
12. Blattner TC, George N, Lee CC, Kumar V, Yelton CDJ. Efficacy of cone-beam computed tomography as a modality to accurately identify the presence of second mesiobuccal canals in maxillary first and second molars: a pilot study. *J Endod*. (2010) **36**:867–70. doi: 10.1016/j.joen.2009.12.023
13. Diogenes A, Simpn S, Law AS. Regenerative endodontics. In: Berman L, Hargreaves K, editors. *Cohen's Pathways of the Pulp*. St Louis: Elsevier (2015). p. 447–73.
14. Idiyatullin D, Corum C, Park JY, Garwood M. Fast and quiet MRI using a swept radiofrequency. *J Magn Reson*. (2006) **181**:342–9. doi: 10.1016/j.jmr.2006.05.014
15. Idiyatullin D, Corum C, Moeller S, Prasad HS, Garwood M, Nixdorf DR. Dental magnetic resonance imaging: making the invisible visible. *J Endod*. (2011) **37**:745–52. doi: 10.1016/j.joen.2011.02.022
16. Feldchtein FI, Gelikonov GV, Gelikonov VM, Iksanov RR, Kuranov R V, Sergeev AM, et al. *In vivo* OCT imaging of hard and soft tissue of the oral cavity. *Opt Express*. (1998) **3**:239–50. doi: 10.1364/OE.3.000239
17. Wilder-Smith P, Otis L, Zhang J, Chen Z. Dental OCT. In: Drexler W, Fujimoto JG, editors. *Optical Coherence Tomography: Technology and Applications*. Berlin: Springer Berlin Heidelberg (2008). p. 1151–82. doi: 10.1007/978-3-540-77550-8_37
18. Machoy M, Seeliger J, Szyszka-Sommerfeld L, Koprowski R, Gedrange T, Wozniak K. The use of optical coherence tomography in dental diagnostics: a state-of-the-art review. *J Healthc Eng*. (2017) **2017**:7560645. doi: 10.1155/2017/7560645
19. de Boer JF, Hitzenberger CK, Yasuno Y. Polarization sensitive optical coherence tomography – a review. *Biomed Opt Express*. (2017) **8**:1838–73. doi: 10.1364/BOE.8.001838
20. de Paula Eduardo C, Aranha ACC, Muller Ramalho K, Bello-Silva MS, de Freitas PM. Laser dentistry research. In: Convissa RA, editor. *Principles and Practice of Laser Dentistry*. Saint Louis: Mosby (2015). p. 303–314. doi: 10.1016/B978-0-323-06206-0.00017-5
21. Contaldo M, Serpico R, Lucchese A. *In vivo* imaging of enamel by reflectance confocal microscopy (RCM): non-invasive analysis of dental surface. *Odontology*. (2014) **102**:325–29. doi: 10.1007/s10266-013-0110-9
22. Contaldo M, Di Stasio D, Santoro R, Laino L, Perillo L, Petruzzi M, et al. Non-invasive *in vivo* visualization of enamel defects by reflectance confocal microscopy (RCM). *Odontology*. (2015) **103**:177–84. doi: 10.1007/s10266-014-0155-4
23. Clark AL, Gillenwater AM, Collier TG, Alizadeh-Naderi R, El-Naggar AK, Richards-Kortum RR. Confocal microscopy for real-time detection of oral cavity neoplasia. *Clin Cancer Res*. (2003) **9**:4714–21. doi: 10.1117/1.1805558
24. Tezuka F. Diagnostic validity and variability of histopathology. *Rinsho Byori*. (1994) **42**:902–6.
25. Chatterjee S. Artefacts in histopathology. *J Oral Maxillofac Pathol*. (2014) **18**:111–6. doi: 10.4103/0973-029X.141346
26. Logan RM, Goss AN. Biopsy of the oral mucosa and use of histopathology services. *Aust Dent J*. (2010) **55**:9–13. doi: 10.1111/j.1834-7819.2010.01194.x
27. Kim J, Lee HS, Song IS, Jung KH. DeNTNet: deep neural transfer network for the detection of periodontal bone loss using panoramic dental radiographs. *Sci Rep*. (2019) **9**:17615. doi: 10.1038/s41598-019-53758-2
28. Flügge T, Hövener JB, Ludwig U, Eisenbeiss AK, Spittau B, Hennig J, et al. Magnetic resonance imaging of intraoral hard and soft tissues using

an intraoral coil and FLASH sequences. *Eur Radiol*. (2016) **26**:4616–23. doi: 10.1007/s00330-016-4254-1
29. Tsai MT, Wang YL, Yeh TW, Lee HC, Chen WJ, Ke JL, et al. Early detection of enamel demineralization by optical coherence tomography. *Sci Rep*. (2019) **9**:17154. doi: 10.1038/s41598-019-53567-7
30. Kosugi A, Kasahara M, Yang L, Nakamura-Takahashi A, Shibahara T, Mori T. Method for diagnosing neoplastic lesions by quantitative fluorescence value. *Sci Rep*. (2019) **9**:7833. doi: 10.1038/s41598-019-44287-z
31. Aubreville M, Knipfer C, Oetter N, Jaremenko C, Rodner E, Denzler J, et al. Automatic classification of cancerous tissue in laserendomicroscopy images of the oral cavity using deep learning. *Sci Rep*. (2017) **7**:11979. doi: 10.1038/s41598-017-12320-8
32. Göppert-Mayer M. Elementary processes with two quantum transitions. *Ann der Phys*. (2009) **18**:466–79. doi: 10.1002/andp.200910358
33. Denk W, Strickler JH, Webb WW. Two-photon laser scanning fluorescence microscopy. *Science*. (1990) **248**:73–6. doi: 10.1126/science.2321027
34. Zipfel WR, Williams RM, Webb WW. Nonlinear magic: multiphoton microscopy in the biosciences. *Nat Biotechnol*. (2003) **21**:1369–77. doi: 10.1038/nbt899
35. Campagnola PJ, Dong CY. Second harmonic generation microscopy: principles and applications to disease diagnosis. *Laser Photonics Rev*. (2011) **5**:13–26. doi: 10.1002/lpor.200910024
36. Mazumder N, Balla NK, Zhuo GY, Kistenev Y V, Kumar R, Kao FJ, et al. Label-free non-linear multimodal optical microscopy—basics, development, and applications. *Front Phys*. (2019) **7**:170. doi: 10.3389/fphy.2019.00170
37. Helmchen F, Denk W. Deep tissue two-photon microscopy. *Nat Methods*. (2005) **2**:932–40. doi: 10.1038/nmeth818
38. Bueno JM, Ávila FJ, Artal P. Comparison of second harmonic microscopy images of collagen-based ocular tissues with 800 and 1045 nm. *Biomed Opt Express*. (2017) **8**:5065–74. doi: 10.1364/BOE.8.005065
39. Masters BR, So PTC. Confocal microscopy and multi-photon excitation microscopy of human skin *in vivo*. *Opt Express*. (2001) **8**:2–10. doi: 10.1364/OE.8.000002
40. Williams RM, Zipfel WR, Webb WW. Multiphoton microscopy in biological research. *Curr Opin Chem Biol*. (2001) **5**:603–8. doi: 10.1016/S1367-5931(00)00241-6
41. Georgakoudi I, Quinn KP. Optical imaging using endogenous contrast to assess metabolic state. *Annu Rev Biomed Eng*. (2012) **14**:351–67. doi: 10.1146/annurev-bioeng-071811-150108
42. Balu M, Zachary CB, Harris RM, Krasieva TB, König K, Tromberg BJ, et al. *In vivo* multiphoton microscopy of basal cell carcinoma. *JAMA Dermatol*. (2015) **151**:1068–74. doi: 10.1001/jamadermatol.2015.0453
43. Horton NG, Wang K, Kobat D, Clark CG, Wise FW, Schaffer CB, et al. *In vivo* three-photon microscopy of subcortical structures within an intact mouse brain. *Nat Photonics*. (2013) **7**:205–9. doi: 10.1038/nphoton.2012.336
44. Suhling K, Hirvonen LM, Levitt JA, Chung PH, Tregidgo C, Le Marois A, et al. Fluorescence lifetime imaging (FLIM): basic concepts and some recent developments. *Med Photonics*. (2015) **27**:3–40. doi: 10.1016/j.medpho.2014.12.001
45. Kolenc OI, Quinn KP. Evaluating cell metabolism through autofluorescence imaging of NAD(P)H and FAD. *Antioxid Redox Signal*. (2019) **30**:875–89. doi: 10.1089/ars.2017.7451
46. Witte S, Negrean A, Lodder JC, De Kock CPJ, Silva GT, Mansvelder HD, et al. Label-free live brain imaging and targeted patching with third-harmonic generation microscopy. *Proc Natl Acad Sci USA*. (2011) **108**:5970–5. doi: 10.1073/pnas.1018743108
47. Zhang Z, de Munck JC, Verburg N, Rozemuller AJ, Vreuls W, Cakmak P, et al. Quantitative third harmonic generation microscopy for assessment of glioma in human brain tissue. *Adv Sci*. (2019) **6**:1900163. doi: 10.1002/advs.201900163
48. Kuzmin NV, Wesseling P, Hamer PC de W, Noske DP, Galgano GD, Mansvelder HD, et al. Third harmonic generation imaging for fast, label-free pathology of human brain tumors. *Biomed Opt Express*. (2016) **7**:1889. doi: 10.1364/BOE.7.001889
49. Lefort C. A review of biomedical multiphoton microscopy and its laser sources. *J Phys D Appl Phys*. (2017) **50**:423001. doi: 10.1088/1361-6463/aa8050
50. Perrin L, Bayarmagnai B, Gligorijevic B. Frontiers in intravital multiphoton microscopy of cancer. *Cancer Rep*. (2020) **3**:e1192. doi: 10.1002/cnr2.1192
51. Klemp M, Meinke MC, Weinigel M, Röwert-Huber HJ, König K, Ulrich M, et al. Comparison of morphologic criteria for actinic keratosis and squamous cell carcinoma using *in vivo* multiphoton tomography. *Exp Dermatol*. (2016) **25**:218–22. doi: 10.1111/exd.12912
52. Ávila FJ, Gambín A, Artal P, Bueno JM. *In vivo* two-photon microscopy of the human eye. *Sci Rep*. (2019) **9**:10121. doi: 10.1038/s41598-019-46568-z
53. Bueno JM, Palacios R, Pennos A, Artal P. Second-harmonic generation microscopy of photocurable polymer intrastromal implants in *ex-vivo* corneas. *Biomed Opt Express*. (2015) **6**:2211–19. doi: 10.1364/BOE.6.002211
54. Ávila FJ, Artal P, Bueno JM. Quantitative discrimination of healthy and diseased corneas with second harmonic generation microscopy. *Transl Vis Sci Technol*. (2019) **8**:51. doi: 10.1167/tvst.8.3.51
55. Bueno JM, Ávila FJ, Martínez-Garciá MC. Quantitative analysis of the corneal collagen distribution after *in vivo* cross-linking with second harmonic microscopy. *Biomed Res Int*. (2019) **2019**:3860498. doi: 10.1155/2019/3860498
56. Kantelhardt SR, Kalasauskas D, König K, Kim E, Weinigel M, Uchugonova A, et al. *In vivo* multiphoton tomography and fluorescence lifetime imaging of human brain tumor tissue. *J Neurooncol*. (2016) **127**:473–82. doi: 10.1007/s11060-016-2062-8
57. Dilipkumar A, Al-Shemmary A, Kreiß L, Cvecek K, Carlé B, Knieling F, et al. Label-free multiphoton endomicroscopy for minimally invasive *in vivo* imaging. *Adv Sci*. (2019) **6**:1801735. doi: 10.1002/advs.201801735
58. Stanciu SG, Xu S, Peng Q, Yan J, Stanciu GA, Welsch RE, et al. Experimenting liver fibrosis diagnostic by two photon excitation microscopy and bag-of-features image classification. *Sci Rep*. (2014) **4**:4636. doi: 10.1038/srep04636
59. Stanciu SG, Ávila FJ, Hristu R, Bueno JM. A study on image quality in polarization-resolved second harmonic generation microscopy. *Sci Rep*. (2017) **7**:15476. doi: 10.1038/s41598-017-15257-0
60. Perry SW, Burke RM, Brown EB. Two-photon and second harmonic microscopy in clinical and translational cancer research. *Ann Biomed Eng*. (2012) **40**:277–91. doi: 10.1007/s10439-012-0512-9
61. Arola DD, Gao S, Zhang H, Masri R. The tooth: its structure and properties. *Dent Clin*. (2017) **61**:651–68. doi: 10.1016/j.cden.2017.05.001
62. Shahmoradi M, Bertassoni LE, Elfallah HM, Swain M. Fundamental structure and properties of enamel, dentin and cementum. In: Ben-Nissan B, editor. *Advances in Calcium Phosphate Biomaterials*. Berlin: Springer Berlin Heidelberg (2014). p. 511–47. doi: 10.1007/978-3-642-53980-0_17
63. Matsumoto-Nakano M. Dental caries. In: *Reference Module in Biomedical Sciences*. Elsevier (2014). Available online at: https://www.sciencedirect.com/science/article/pii/B9780128012383000015?via%3Dihub
64. Kao F-J, Wang Y-S, Huang M-K, Huang S-L, Cheng PC. Second-harmonic generation microscopy of tooth. *Opt Sensing Imaging Manip Biol Biomed Appl*. (2000) **4082**:119. doi: 10.1117/12.390534
65. Fu-Jen K, Chin-Ying SH. "Harmonic generation microscopy of dental sections," *Proc. SPIE 5630, Optics in Health Care and Biomedical Optics: Diagnostics and Treatment II* (2005). doi: 10.1117/12.577285
66. Kao F-J. The use of optical parametric oscillator for harmonic generation and two-photon uv fluorescence microscopy. *Microsc Res Tech*. (2004) **63**:175–81. doi: 10.1002/jemt.20026
67. Chen M-H, Chen W-L, Sun Y, Fwu PT, Lin M-G, Dong C-Y. Three-dimensional tooth imaging using multiphoton and second harmonic generation microscopy. *Lasers Dent XIII*. (2007) **6425**:642503. doi: 10.1117/12.698840
68. Chen M-H, Chen W-L, Sun Y, Fwu PT, Dong C-Y. Multiphoton autofluorescence and second-harmonic generation imaging of the tooth. *J Biomed Opt*. (2007) **12**:064018. doi: 10.1117/1.2812710
69. Bueno JM, Martínez-Ojeda RM, Ávila FJ, Fernández-Escudero AC, López-Nicolás M, Pérez-Carceles MD. Multiphoton imaging microscopy of dental pieces as a tool in forensic sciences. In: *Program and Abstract Book Focus on Microscopy 2019*. London (2009). p. 266.
70. Elbaum R, Tal E, Perets AI, Oron D, Ziskind D, Silberberg Y, et al. Dentin micro-architecture using harmonic generation microscopy. *J Dent*. (2007) **35**:150–5. doi: 10.1016/j.jdent.2006.07.007

71. Chen S-Y, Hsu C-YS, Sun C-K. Epi-third and second harmonic generation microscopic imaging of abnormal enamel. *Opt Express*. (2008) **16**:11670–9. doi: 10.1364/OE.16.011670
72. Cloitre T, Panayotov IV, Tassery H, Gergely C, Levallois B, Cuisinier FJG. Multiphoton imaging of the dentine-enamel junction. *J Biophotonics*. (2013) **6**:330–7. doi: 10.1002/jbio.201200065
73. Pan PY, Chen RS, Ting CL, Chen WL, Dong CY, Chen MH. Multiphoton microscopy imaging of developing tooth germs. *J Formos Med Assoc*. (2014) **113**:42–9. doi: 10.1016/j.jfma.2012.03.016
74. Aboulfadl H, Hulliger J. Absolute polarity determination of teeth cementum by phase sensitive second harmonic generation microscopy. *J Struct Biol*. (2015) **192**:67–75. doi: 10.1016/j.jsb.2015.08.011
75. Wang Z, Zheng W, Stephen Hsu CY, Huang Z. Epi-detected quadruple-modal nonlinear optical microscopy for label-free imaging of the tooth. *Appl Phys Lett*. (2015) **106**:033701. doi: 10.1063/1.4906447
76. Wang Z, Zheng W, Lin J, Hsu C-Y, Huang Z. Integrated coherent raman scattering and multiphoton microscopy for label-free imaging of the dentin in the tooth. *Multiphot Microsc Biomed Sci XIV*. (2014) **8948**:89482N. doi: 10.1117/12.2039683
77. Pezacki JP, Blake JA, Danielson DC, Kennedy DC, Lyn RK, Singaravelu R. Chemical contrast for imaging living systems: molecular vibrations drive CARS microscopy. *Nat Chem Biol*. (2011) **7**:137–45. doi: 10.1038/nchembio.525
78. Traphagen SB, Fourligas N, Xylas JF, Sengupta S, Kaplan DL, Georgakoudi I, et al. Characterization of natural, decellularized and reseeded porcine tooth bud matrices. *Biomaterials*. (2012) **33**:5287–96. doi: 10.1016/j.biomaterials.2012.04.010
79. Atmeh AR, Chong EZ, Richard G, Boyde A, Festy F, Watson TF. Calcium silicate cement-induced remineralisation of totally demineralised dentine in comparison with glass ionomer cement: tetracycline labelling and two-photon fluorescence microscopy. *J Microsci*. (2015) **257**:151–60. doi: 10.1111/jmi.12197
80. Chen Y-C, Lee S-Y, Wu Y, Brink K, Shieh D-B, Huang TD, et al. Third-harmonic generation microscopy reveals dental anatomy in ancient fossils. *Opt Lett*. (2015) **40**:1354–7. doi: 10.1364/OL.40.001354
81. Girkin JM, Hall AF, Creanor SL. Multi-photon imaging of intact dental tissue. In: *Proceedings of the 4th Annual Indiana Conference*. Indianapolis (1999). p. 155–168.
82. Girkin JM, Hall AF, Creanor SL. Two-photon imaging of intact dental tissue. *Dent Caries*. (2000) **2**:317–25.
83. Girkin JM. Optical physics enables advances in multiphoton imaging. *J Phys D Appl Phys*. (2003) **36**:R250–8. doi: 10.1088/0022-3727/36/14/204
84. Hall A, Girkin JM. A review of potential new diagnostic modalities for caries lesions. *J Dent Res*. (2004) **83**:89–94. doi: 10.1177/154405910408301s18
85. Lin P-Y, Lyu H-C, Hsu C-YS, Chang C-S, Kao F-J. Imaging carious dental tissues with multiphoton fluorescence lifetime imaging microscopy. *Biomed Opt Express*. (2011) **2**:149–58. doi: 10.1364/BOE.2.000149
86. Terrer E, Panayotov IV, Slimani A, Tardivo D, Gillet D, Levallois B, et al. Laboratory studies of nonlinear optical signals for caries detection. *J Dent Res*. (2016) **95**:574–9. doi: 10.1177/0022034516629400
87. Slimani A, Tardivo D, Panayotov IV, Levallois B, Gergely C, Cuisinier F, et al. Multiphoton microscopy for caries detection with ICDAS classification. *Caries Res*. (2018) **52**:359–66. doi: 10.1159/000486428
88. Trunina NA, Popov AP, Lademann J, Tuchin VV, Myllylä R, Darvin ME. Two-photon-excited autofluorescence and second-harmonic generation microscopy for the visualization of penetration of TiO 2 and ZnO nanoparticles into human tooth tissue *ex vivo*. *Biophoton Photon Solut Better Heal Care III*. (2012) **8427**:84270Y. doi: 10.1117/12.924073
89. Trunina NA, Darvin ME, Kordas K, Sarkar A, Mikkola JP, Lademann J, et al. Monitoring of TiO 2 and ZnO nanoparticle penetration into enamel and dentine of human tooth *in vitro* and assessment of their photocatalytic ability. *IEEE J Sel Top Quantum Electron*. (2014) **20**:133–40. doi: 10.1109/JSTQE.2013.2276082
90. Maber M, Liversidge HM, Hector MP. Accuracy of age estimation of radiographic methods using developing teeth. *Forensic Sci Int*. (2006) **159**:S68–73. doi: 10.1016/j.forsciint.2006.02.019
91. Ingrams DR, Dhingra JK, Roy K, Perrault DF, Bottrill ID, Kabani S, et al. Autofluorescence characteristics of oral mucosa. *Head Neck*. (1997) **19**:27–32.
92. Vargas G, Shilagard T, Ho KH, McCammon S. Multiphoton autofluorescence microscopy and second harmonic generation microscopy of oral epithelial neoplasms. In: *Proceedings of the 31st Annual International Conference of the IEEE Engineering in Medicine and Biology Society: Engineering the Future of Biomedicine, EMBC 2009*, St. Paul: Minneapolis (2009). p. 6311–3.
93. Wilder-Smith P, Osann K, Hanna N, El Abbadi N, Brenner M, Messadi D, et al. *In vivo* multiphoton fluorescence imaging: a novel approach to oral malignancy. *Lasers Surg Med*. (2004) **35**:96–103. doi: 10.1002/lsm.20079
94. Wilder-Smith P, Krasieva T, Jung W-G, Zhang J, Chen Z, Osann K, et al. Noninvasive imaging of oral premalignancy and malignancy. *J Biomed Opt*. (2005) **10**:051601. doi: 10.1117/1.2098930
95. Wu Y, Qu JY. Two-photon autofluorescence spectroscopy and second-harmonic generation of epithelial tissue. *Opt Lett*. (2005) **30**:3045. doi: 10.1364/OL.30.003045
96. Skala MC, Riching KM, Gendron-Fitzpatrick A, Eickhoff J, Eliceiri KW, White JG, et al. *In vivo* multiphoton microscopy of NADH and FAD redox states, fluorescence lifetimes, and cellular morphology in precancerous epithelia. *Proc Natl Acad Sci USA*. (2007) **104**:19494–9. doi: 10.1073/pnas.0708425104
97. Hristu R, Stanciu SG, Tranca DE, Stanciu GA. Improved quantification of collagen anisotropy with polarization-resolved second harmonic generation microscopy. *J Biophotonics*. (2017) **10**:1171–9. doi: 10.1002/jbio.201600197
98. Zhuo S, Chen J, Jiang X, Xie S, Chen R, Cao N, et al. The layered-resolved microstructure and spectroscopy of mouse oral mucosa using multiphoton microscopy. *Phys Med Biol*. (2007) **52**:4967–80. doi: 10.1088/0031-9155/52/16/017
99. Tsai M-R, Chen S-Y, Shieh D-B, Lou P-J, Sun C-K. *In vivo* optical virtual biopsy of human oral mucosa with harmonic generation microscopy. *Biomed Opt Express*. (2011) **2**:2317–28. doi: 10.1364/BOE.2.002317
100. Miri AK, Tripathy U, Mongeau L, Wiseman PW. Nonlinear laser scanning microscopy of human vocal folds. *Laryngoscope*. (2012) **122**:356–63. doi: 10.1002/lary.22460
101. Heris HK, Miri AK, Ghattamaneni NR, Li NYK, Thibeault SL, Wiseman PW, et al. Microstructural and mechanical characterization of scarred vocal folds. *J Biomech*. (2015) **48**:708–11. doi: 10.1016/j.jbiomech.2015.01.014
102. Yildirim M, Quinn KP, Kobler JB, Zeitels SM, Georgakoudi I, Ben-Yakar A. Quantitative differentiation of normal and scarred tissues using second-harmonic generation microscopy. *Scanning*. (2016) **38**:684–93. doi: 10.1002/sca.21316
103. Kazarine A, Kolosova K, Gopal AA, Wang H, Tahara R, Rammal A, et al. Multimodal virtual histology of rabbit vocal folds by nonlinear microscopy and nano computed tomography. *Biomed Opt Express*. (2019) **10**:1151. doi: 10.1364/BOE.10.001151
104. Sriram G, Sudhaharan T, Wright GD. Multiphoton microscopy for noninvasive and label-free imaging of human skin and oral mucosa equivalents. In: *Methods in Molecular Biology*. Totowa, NJ: Humana Press (2019). p. 1–18.
105. Scully C, Bagan J. Oral squamous cell carcinoma overview. *Oral Oncol*. (2009) **45**:301–8. doi: 10.1016/j.oraloncology.2009.01.004
106. Lumerman H, Freedman P, Kerpel S. Oral epithelial dysplasia and the development of invasive squamous cell carcinoma. *Oral Surg Oral Med Oral Pathol Oral Radiol Endod*. (1995) **79**:321–9. doi: 10.1016/S1079-2104(05)80226-4
107. Karabut M, Kiseleva EB, Sirotkina MA, Kuznetsov SS, Matveev LA, Moiseev AA, et al. Multiphoton tomography and multimodal OCT for *in vivo* visualization of oral malignancy in the hamster cheek pouch. *Photonic Solut Better Heal Care VI*. (2018) **10685**:1–8. doi: 10.1117/12.2306210
108. Gatesman Ammer A, Hayes KE, Martin KH, Zhang L, Spirou GA, Weed SA. Multi-photon imaging of tumor cell invasion in an orthotopic mouse model of oral squamous cell carcinoma. *J Visualized Experiments: JoVE* (2011) 2941. doi: 10.3791/2941
109. Edward K, Shilagard T, Qiu S, Vargas G. Two-photon autofluorescence spectroscopy of oral mucosa tissue. *Multiphot Microsc Biomed Sci XI*. (2011) **7903**:79031Q. doi: 10.1117/12.875049

110. Pal R, Edward K, Ma L, Qiu S, Vargas G. Spectroscopic characterization of oral epithelial dysplasia and squamous cell carcinoma using multiphoton autofluorescence micro-spectroscopy. *Lasers Surg Med*. (2017) **49**:866–73. doi: 10.1002/lsm.22697
111. Motamedi S, Shilagard T, Koong L, Vargas G. Feasibility of using gold nanorods for optical contrast in two photon microscopy of oral carcinogenesis. *Proc SPIE 7576, Reporters, Markers, Dyes, Nanoparticles, and Molecular Probes for Biomedical Applications II* (2010) 75760Z. doi: 10.1117/12.843036
112. Motamedi S, Shilagard T, Edward K, Koong L, Qui S, Vargas G. Gold nanorods for intravital vascular imaging of preneoplastic oral mucosa. *Biomed Opt Express*. (2011) **2**:1194. doi: 10.1364/BOE.2.001194
113. Olesiak-Banska J, Waszkielewicz M, Obstarczyk P, Samoc M. Two-photon absorption and photoluminescence of colloidal gold nanoparticles and nanoclusters. *Chem Soc Rev*. (2019) **48**:4087–117. doi: 10.1039/C8CS00849C
114. Tsai MR, Shieh D Bin, Lou PJ, Lin CF, Sun CK. Characterization of oral squamous cell carcinoma based on higher-harmonic generation microscopy. *J Biophotonics*. (2012) **5**:415–24. doi: 10.1002/jbio.201100144
115. Cheng Y-H, Lin C-F, Shih T-F, Sun C-K. A novel intravital multi-harmonic generation microscope for early diagnosis of oral cancer. *Opt Biopsy XI*. (2013) **8577**:85770R. doi: 10.1117/12.2001593
116. Sun Y, Phipps J, Elson DS, Stoy H, Tinling S, Meier J, et al. Fluorescence lifetime imaging microscopy: *in vivo* application to diagnosis of oral carcinoma. *Opt Lett*. (2009) **34**:2081. doi: 10.1364/OL.34.002081
117. Shah AT, Skala MC. *Ex vivo* label-free microscopy of head and neck cancer patient tissues. *Multiphot Microsc Biomed Sci XV*. (2015) **9329**:93292B. doi: 10.1117/12.2075583
118. Teh SK, Zheng W, Li S, Li D, Zeng Y, Yang Y, et al. Multimodal nonlinear optical microscopy improves the accuracy of early diagnosis of squamous intraepithelial neoplasia. *J Biomed Opt*. (2013) **18**:036001. doi: 10.1117/1.JBO.18.3.036001
119. Huttunen MJ, Hristu R, Dumitru A, Floroiu I, Costache M, Stanciu SG. Multiphoton microscopy of the dermoepidermal junction and automated identification of dysplastic tissues with deep learning. *Biomed Opt Express*. (2020) **11**:186. doi: 10.1364/BOE.11.000186
120. Rivenson Y, Wang H, Wei Z, de Haan K, Zhang Y, Wu Y, et al. Virtual histological staining of unlabelled tissue-autofluorescence images via deep learning. *Nat Biomed Eng*. (2019) **3**:466. doi: 10.1038/s41551-019-0362-y

Conflict of Interest: The authors declare that the research was conducted in the absence of any commercial or financial relationships that could be construed as a potential conflict of interest.